



HAL
open science

Concurrent Jovian S-Burst Beaming as Observed From LWA1, NDA, and Ukrainian Radio Telescopes

Masafumi Imai, Alain Lecacheux, Tracy E. Clarke, Charles A. Higgins,
Mykhaylo Panchenko, Vyacheslav V. Zakharenko, Anatolii I. Brazhenko,
Anatolii V. Frantsuzenko, Oleg N. Ivantyshin, Alexandr A. Konovalenko, et al.

► **To cite this version:**

Masafumi Imai, Alain Lecacheux, Tracy E. Clarke, Charles A. Higgins, Mykhaylo Panchenko, et al..
Concurrent Jovian S-Burst Beaming as Observed From LWA1, NDA, and Ukrainian Radio Telescopes.
Journal of Geophysical Research Space Physics, 2019, 124, pp.5302-5316. 10.1029/2018JA026445 .
insu-03717029

HAL Id: insu-03717029

<https://insu.hal.science/insu-03717029>

Submitted on 8 Jul 2022

HAL is a multi-disciplinary open access archive for the deposit and dissemination of scientific research documents, whether they are published or not. The documents may come from teaching and research institutions in France or abroad, or from public or private research centers.

L'archive ouverte pluridisciplinaire **HAL**, est destinée au dépôt et à la diffusion de documents scientifiques de niveau recherche, publiés ou non, émanant des établissements d'enseignement et de recherche français ou étrangers, des laboratoires publics ou privés.

Copyright

JGR Space Physics

RESEARCH ARTICLE

10.1029/2018JA026445

Key Points:

- S-burst long baseline analysis was performed using five powerful radio telescopes on the ground
- Statistics of nine Io-related events show that S-burst beam is formed by a flashlight-like beam structure
- The cross-correlation analysis can isolate the S-burst frequency-dependent distributions from those of the other emissions

Correspondence to:

M. Imai,
 masafumi-imai@uiowa.edu

Citation:

Imai, M., Lecacheux, A., Clarke, T. E., Higgins, C. A., Panchenko, M., Zakharenko, V. V., et al. (2019). Concurrent Jovian S-burst beaming as observed from LWA1, NDA, and Ukrainian radio telescopes. *Journal of Geophysical Research: Space Physics*, 124, 5302–5316. <https://doi.org/10.1029/2018JA026445>






Received 24 DEC 2018

Accepted 20 JUN 2019

Accepted article online 4 JUL 2019

Published online 13 JUL 2019

Concurrent Jovian S-Burst Beaming as Observed From LWA1, NDA, and Ukrainian Radio Telescopes

Masafumi Imai¹ , Alain Lecacheux², Tracy E. Clarke³ , Charles A. Higgins⁴, Mykhaylo Panchenko⁵ , Vyacheslav V. Zakharenko⁶ , Anatolii I. Brazhenko⁷, Anatolii V. Frantsuzenko⁷, Oleg N. Ivantyshin⁸, Alexandr A. Konovalenko⁶, and Volodymyr V. Koshovyy⁸ 

¹Department of Physics and Astronomy, University of Iowa, Iowa City, IA, USA, ²Laboratoire d'Etudes Spatiales et d'Instrumentation en Astrophysique, CNRS/Observatoire de Paris, Meudon, France, ³Naval Research Laboratory, Washington, DC, USA, ⁴Department of Physics and Astronomy, Middle Tennessee State University, Murfreesboro, TN, USA, ⁵Space Research Institute, Austrian Academy of Sciences, Graz, Austria, ⁶Institute of Radio Astronomy, National Academy of Sciences of Ukraine, Kharkiv, Ukraine, ⁷Poltava Gravimetric Observatory, S. Subotin Institute of Geophysics, National Academy of Sciences of Ukraine, Poltava, Ukraine, ⁸Karpenko Physico-Mechanical Institute, National Academy of Sciences of Ukraine, Lviv, Ukraine

Abstract This paper describes the statistical property of Jupiter's millisecond burst (S-burst) beaming for Io-related decametric (Io-DAM) sources from a ground-based radio telescope network. To do so, we performed simultaneous observations of Jovian Io-DAM S-bursts from 15 January through 4 May 2016 for a total of nine events using several radio telescopes. These radio telescopes include the Long Wavelength Array station One (LWA1) in the United States, Nançay Decameter Array (NDA) in France, and three large radio telescopes (UTR2, URAN2, and URAN3) in Ukraine. We conducted a cross-correlation analysis of the S-burst spectrograms in a frequency range of 10.5 to 33 MHz over effective baselines of up to 8,950 km. We found that the beaming of the S-bursts is formed on the flashlight-like structure within an east-west beam width of 2.75" for Io-A/C, 2.63" for Io-A', and 2.75" for Io-B/D. In parallel, the flashlight-like beam was completely filled because the results from all usable pairs of telescopes supported this model. Hence, these beam widths directly correspond to the minimum cone thickness where a radio source emanates over large solid angles from the same direction of Jupiter, as opposed to a localized radio source emitting over small solid angles along active magnetic flux tubes that are tied to Io's orbital motion in Jupiter's rotation frame (beacon-like structure). Additionally, this cross-correlation technique shows a practical benefit of producing statistical profiles of S-bursts.

Plain Language Summary In our solar system, Jupiter is second only to the Sun in its intensity as a radio source. One of the radio sources tied to Jovian auroras dominates at the decameter wavelength, exhibiting fine structures (called S-bursts) in a timescale of milliseconds. While spacecraft equipped with a low-frequency radio system is insufficient to capture S-bursts in a broad frequency bandwidth and a long-term period, Earth-based radio telescopes offer high-resolution observations of Jovian S-bursts. Using five world-class large radio telescopes in the United States, France, and Ukraine, we performed the common S-burst observation campaign in 2016. We found that S-burst beaming is wide enough to cover the maximum baseline of 8,950 km between radio telescopes in the United States and Ukraine. This result provides a nature of Jovian S-burst beaming lasting on the order of the milliseconds.

1. Introduction

The fortuitous detection of Jovian decametric (DAM) radiation from a terrestrial observer in 1955 (Burke & Franklin, 1955) proved the existence of magnetic fields at a planet other than Earth. The sources of this nonthermal DAM emission are distributed along auroral magnetic field lines at emission frequencies very close to the local gyrofrequencies via the electron cyclotron maser instability (CMI; Wu & Lee, 1979). Jovian DAM radiation above 10 MHz is readily observed by Earth-based radio telescopes that are limited at lower frequencies by terrestrial ionospheric conditions and radio frequency interference. This sporadic DAM emission extends in a broad frequency range from a few to 40 MHz, reaches a flux density of 10^{-21} to

10^{-20} W/(m² Hz) at 4 AU, and has strongly elliptical polarization (Carr et al., 1983; Clarke et al., 2004; Zarka, 1998, and references therein).

The morphology of Jovian DAM radiation can be divided into short-burst (S-burst) and long-burst (L-burst; Gallet, 1961). In the dynamic spectra, S-bursts present both simple and complex structures on the order of milliseconds, appearing at narrow Io phases around 90° and 240°, where the Io phase is an orbital angle between the observer and the Jovian moon Io from superior conjunction. These specific regions originating from these S-bursts are Io-related DAM (Io-DAM) sources owing to the intense interaction of Jupiter and Io (Bigg, 1964). In contrast, L-bursts exhibit arc-like spectral shapes changing on timescale of seconds to minutes, accompanied by Faraday fringes (Warwick & Dulk, 1964), interplanetary scintillation, and modulation lanes (Riihimaa, 1968). These L-bursts are ubiquitous at all Io phases including both Io-DAM sources and non-Io-related DAM sources.

The Io-DAM sources comprise the right-hand polarized Io-A and Io-B sources emanating from Jupiter's northern hemisphere and the left-hand polarized Io-C and Io-D sources from the southern hemisphere. Jovian Io-DAM emission is the right-hand extraordinary (R-X) mode wave and has a hollow cone beam, in which the half-angle of cone is measured between a magnetic field vector at the apex of a radio source and the wave vector \mathbf{k} (Dulk, 1970). This hollow cone Io-DAM emission is swept from the Io-B and Io-D sources on the Jovian dawnside to the Io-A and Io-C sources on the duskside as viewed from Earth. Another well-known source is the Io-A' source with the right-hand polarization similar to the Io-A source, but the spectral morphology is different (Leblanc, 1981). This difference of the sources is easily distinguishable in the diagram of Jovian radio occurrence probability as a function of Jupiter's System III central meridian longitude (CML) and Io phase.

The first long baseline interferometer observation of Jovian DAM radiation was made with a narrowband receiver at 19.6 MHz over a north-south 32.3 km baseline in 1962 (Slee & Higgins, 1963). Since then, single-frequency long baseline analyses were performed with various baselines from 17 km through 7,500 km to constrain Jovian radio source size and beam thickness at 18 MHz (Brown et al., 1968; Carr et al., 1970; Lynch et al., 1972, 1976; Phillips et al., 1988), 19.6 MHz (Slee & Higgins, 1966), and 34 MHz (Dulk, 1970; Dulk et al., 1967; Stannard et al., 1970). Among the earlier studies, Dulk (1970) performed the first very long baseline interferometry (VLBI) measurements of S-bursts over a 4,300-km north-south baseline, and Carr et al. (1970) and Lynch et al. (1976) extended to a north-south baseline up to 7,500 and 6,980 km, respectively. They concluded that the upper bound of radio source size is either 0.1" (400 km at Jupiter) as an incoherent source or 1" (4,000 km) as a coherent source. Also, Lynch et al. (1976) reported that the direction of arrival of the 68 S-burst analyzed is all the same within a 1.8" north-south view of the interferometers (i.e., 1.8" minimum beaming thickness). However, the earlier studies have difficulty monitoring the spectral variations of broad S-burst spectra over a long-term period.

With the aid of technical advances in radio arrays and wide-band receivers, high sensitivity and broad dynamic range long baseline interferometers for Jovian S-bursts have been demonstrated with several powerful radio telescopes since late 1990s (Imai et al., 2016; Lecacheux et al., 2004; Nigl et al., 2007; Rucker et al., 2001). These radio telescopes include the UTR2 and URAN2 in Ukraine, Nançay Decameter Array (NDA) in France, the initial test station of Low-Frequency Array (LOFAR/ITS) in the Netherlands, and Long Wavelength Array station One (LWA1) in the United States. Rucker et al. (2001) and Lecacheux et al. (2004) analyzed a few of the synchronized S-burst dynamic spectra from 22 to 26 MHz, finding good correlation of the spectra between UTR2 and NDA, about 3,000 km apart. By investigating S-burst VLBI observations from 20 to 25 MHz with LOFAR/ITS and NDA, Nigl et al. (2007) showed that S-bursts have no temporal change of high correlations and fringe visibility of 1 in a few seconds. This result was interpreted to indicate that the S-burst sources are smaller than the angular resolution 4" (702-km distance at 25 MHz), consistent with the previous estimate of 0.1" to 1". source size (Carr et al., 1970; Dulk, 1970; Lynch et al., 1976).

Recently, Imai et al. (2016) have, using a cross-correlation analysis, examined the lag times of a 105-min Jovian Io-D/B S-burst event in a frequency range of 10 to 33 MHz from LWA1, NDA, and URAN2 over effective baselines of up to 8,460 km. They found that the trend of the lag times with high correlations between the spectra correspond to the rotational motion of the observers on Earth, not S-burst radio sources on Jupiter, thereby constraining a minimum thickness of the emission up to 2.66". However, this

observational result was based on only one event study and it remained a question of whether this conclusion is widely acceptable for the other Io-DAM S-burst events.

While most of the previous studies including Imai et al. (2016) analyzed the Jovian Io-D/B radio sources that abound with strong S-bursts, there is little information on the S-burst beaming for the other Io-DAM sources and their statistical beam properties in wide frequencies. Each Io-DAM source exhibits different spectral morphology, entangled with the emission beam geometry, and originates from different System III location owing to the complex Jovian internal magnetic field model (Connerney et al., 2018). Furthermore, the Io-B and Io-D sources are located on the Jovian dawnside and the Io-A and Io-C sources are on the duskside. Therefore, it is worth testing to measure each beam pattern and thickness by performing the cross-correlation analysis of Jovian S-bursts commonly observed from multiple radio telescopes with various baselines.

In this paper, we expand the cross-correlation analysis of Jovian S-burst spectrograms over effective baselines of up to 8,950 km using the above three radio telescopes and two additional radio telescopes UTR2 and URAN3 in Ukraine for a total of nine Jovian Io-DAM S-burst radio events in 2016. Simultaneous observations with these two redundant radio telescopes increase a number of usable baselines (or measurable, angular resolution for Jovian radio beam) via our two-station cross-correlation analysis. This merit allows us to address whether the S-burst beam is filled or hollow and how wide the S-burst beam expands as viewed from Earth. In section 2, we describe the radio receiver and antenna system for each ground-based radio station, the methodology of the cross-correlation analysis, and its results. Section 3 presents the interpretation of the S-burst cross-correlations and exemplifies the statistical distribution of the Io-C event in a frequency of 11 to 33 MHz. Finally, we conclude the results of the S-burst beaming studies and comment on a future prospect with multiobservers for Jovian S-bursts in section 4.

2. Observations and Analysis

Following the successful, initial coordination of Jovian S-burst observations in 2015 (Imai et al., 2016), we have extended coordinated Jovian radio observations with five powerful low-frequency radio telescopes in the United States, France, and Ukraine from 15 January to 4 May 2016. These observations were also a part of global Juno-supporting Jupiter observation campaign during its approach phase to the planet (Bolton et al., 2017). The westernmost of the five telescopes is the LWA1 on the Plains of San Agustin, New Mexico, United States, consisting of 256 bow tie dipoles (Ellingson et al., 2013; Taylor et al., 2012). One of the LWA1 operation modes used in this study is the DRX mode, recording the waveform at two tunings that are selectable for each center frequency in a range of 10 to 88 MHz but fixed with a total bandwidth of 19.6 MHz (Clarke et al., 2014). The waveform is, using the Fourier transform postprocessing, converted into the spectral data with temporal resolution 0.8 ms and spectral resolution 4.79 kHz (Dowell et al., 2012). At the central location of the telescopes, the NDA is located in Nançay, France, comprising 144 conical helices (Boischot et al., 1980; Lecacheux, 2000). Various kinds of spectrometers are installed in NDA, but we use the “Routine” spectrometer that covers the 100-MHz frequency band in an interval of 48.83 kHz and 5 ms. The easternmost of the telescopes situated in Ukraine is the UTR2 in Kharkiv and two subsystems of the four URAN interferometers (URAN2 in Poltava and URAN3 in Lviv) in descending order of a number of dipole antennas (Brazhenko et al., 2005; Konovalenko et al., 2016). These three Ukrainian radio telescopes utilize the common DPS-Z spectrometer (Ryabov et al., 2010; Zakharenko et al., 2016), being capable of recording a radio spectrum of 8 to 33 MHz in a 4.03-kHz interval. The temporal sampling is 0.99 ms for URAN2 and 4.96 ms for the UTR2 and URAN3. Although all radio telescopes but UTR2 have the ability to collect circular and linear polarizations (Stokes V, U, and Q), we use total intensity (Stokes I) throughout this paper. During the Jovian S-burst observation campaign, each ground-based radio station monitored the DAM emissions in overlapping frequencies of 10.5 to 33 MHz with the sampling time of 0.8 to 5 ms. The locations and instrument profiles of the five radio telescopes are summarized in Figure 1a and Table 1.

Table 2 shows the observational and geometrical properties for a total of nine Io-DAM events analyzed in this study, containing a series of S-bursts. These events are also plotted as a function of Jovian CML and Io phase in Figure 1b. Among them, one event was collected from all five telescopes, six events from all but UTR2, and two events from the LWA1, NDA, and URAN2. The east-west angular size θ is a separation angle in the east-west direction at two telescopes on Jovian CML of System III and the effective distance D is a separation distance between two telescopes as seen from Jupiter. Given that \mathbf{a} and \mathbf{b} are the vectors of two

(a) Locations of Earth-Based Low-Frequency Radio Telescopes

(b) Analyzed Observation Coverages

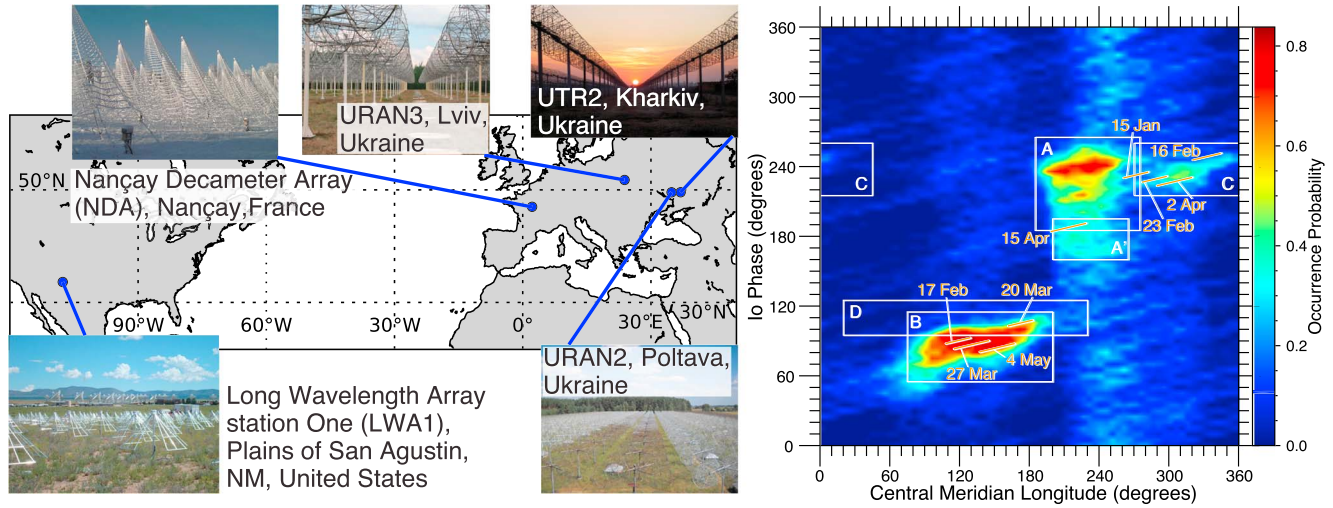


Figure 1. (a) The geometrical configurations of the Long Wavelength Array station One (LWA1), Nançay Decameter Array (NDA), URAN3, URAN2, and UTR2 in eastern sequence. (b) Superimposed with a Jovian radio occurrence probability map at 10–40 MHz using the 13-year NDA synoptic observations (Leblanc et al., 1981, 1983, 1989, 1990, 1993), Earth locations during nine Io-related coordinated observations in 2016 displayed as a function of Io phase and Jovian central meridian longitude. The boundaries of the white boxes correspond to the 10% occurrence probabilities of Io-A, Io-A', Io-B, Io-C, and Io-D at 10–40 MHz based on the 26-year observations from NDA (Marques et al., 2017).

individual telescopes to the center of Jupiter in geocentric cartesian coordinates (Earth centered, Earth fixed coordinates),

$$\theta[\text{rad}] = \arcsin \left(\frac{[\mathbf{a}, \mathbf{b}]_2}{|\mathbf{a}| \cdot |\mathbf{b}|} \right), \quad (1)$$

$$D = \min (|\mathbf{a}|, |\mathbf{b}|) \cdot \theta[\text{rad}] \quad (2)$$

where $[\mathbf{a}, \mathbf{b}]_2$ is the second component of the cross product between \mathbf{a} and \mathbf{b} . The largest values of θ and D are given in a pair of either LWA1-UTR2 or LWA1-URAN2, whichever is available. During the coordinated nine Io-DAM observations, the maximum values range from 2.42" to 2.75" for θ_{\max} in arcseconds and vary in the D_{\max} range of 8,560 to 8,950 km. In contrast, the minimum values are 0.01" to 0.39" for θ_{\min} and 20 to 1,300 km for D_{\min} .

The cross-correlation analysis of the S-burst spectrograms in a short period is a powerful tool to disentangle the beam shape and thickness (Imai et al., 2016; Lecacheux et al., 2004; Nigl et al., 2007; Rucker et al., 2001), as opposed to the fringe visibility and phase information derived from the VLBI data analysis for estimates of the Jovian S-burst source size (Brown et al., 1968; Carr et al., 1970; Dulk, 1970; Dulk et al., 1967; Lynch

Table 1
An Overview of Five Radio Telescopes Used in This Study

| Telescope | Number of antennas × polarization | Operating frequency (MHz) | Receivers/ modes | Temporal resolution (ms) | Spectral resolution (kHz) | Geographical Distance from LWA1 (km) |
|-----------|--------------------------------------|------------------------------|---------------------|-----------------------------|------------------------------|---|
| LWA1 | 256 × 2 | 10–88 | DRX ^a | 0.84 | 4.79 | 0 |
| NDA | 72 × 2 | 10–100 | Routine | 1.0 | 48.8 | 8,600 |
| URAN3 | 256 × 2 | 8–33 | DSP-Z | 4.96 | 4.03 | 9,400 |
| URAN2 | 512 × 2 | 8–33 | DSP-Z | 0.99 | 4.03 | 10,000 |
| UTR2 | (1440 + 600) ^b × 1 | 8–33 | DSP-Z | 4.96 | 4.03 | 10,100 |

Note. LWA1 = Long Wavelength Array station One; NDA = Nançay Decameter Array.

^aThe DRX mode is the waveform recording, having its ability to ultimately convert into the spectrum with 0.21 ms (Dowell et al., 2012). ^bThe former and latter values mean the number of dipole antennas in the north-south and west arms. In this study, we use only the west arms because such a broad antenna beam can cover Jupiter but is less sensitive above 21 MHz at a low elevation of 9° to 16°.

Table 2
Coordinated S-Burst Observation Events Analyzed in This Study

| Io-DAM source region | Date | Start time (UTC) | Duration (s) | Coordinated telescopes ^b | Common frequency (MHz) | Minimum east-west angular size ^b θ_{\min} (") | Minimum effective baseline ^b D_{\min} (km) | Maximum east-west angular size ^b θ_{\max} (") | Maximum effective baseline ^b D_{\max} (km) |
|----------------------|------------------|------------------|--------------|-------------------------------------|---------------------------|---|---|---|---|
| Io-A/C | 15 January 2016 | 06:20:00 | 2,100 | L, N, U2, and U3 | 16.5–33 | 0.14–0.11 | 480–380 | 2.54–2.50 | 8,910–8,790 |
| Io-C | 16 February 2016 | 04:05:00 | 2,400 | L, N, U2, U3, and UT | 10.5/16.5–33 ^c | 0.02–0.01 | 50–20 | 2.74–2.69 | 8,950–8,780 |
| Io-B | 17 February 2016 | 04:00:00 | 2,100 | L, N, U2, and U3 | 20.25–33 | 0.15–0.12 | 480–380 | 2.73–2.69 | 8,900–8,790 |
| Io-A/C | 23 February 2016 | 03:35:00 | 2,100 | L, N, U2, and U3 | 18.25–33 | 0.15–0.12 | 480–380 | 2.75–2.71 | 8,900–8,780 |
| Io-B/D | 20 March 2016 | 01:35:00 | 2,100 | L, N, U2, and U3 | 20.25–33 | 0.15–0.12 | 490–390 | 2.75–2.72 | 8,880–8,790 |
| Io-B | 27 March 2016 | 01:00:30 | 3,000 | L, N, U2, and U3 | 20.25–33 | 0.16–0.11 | 500–360 | 2.73–2.68 | 8,870–8,710 |
| Io-C | 2 April 2016 | 00:45:00 | 3,000 | L, N, U2, and U3 | 18.25–33 | 0.15–0.10 | 480–330 | 2.70–2.63 | 8,870–8,620 |
| Io-A' | 15 April 2016 | 23:40:00 | 3,000 | L, N, and U2 | 18.25–33 | 0.39–0.25 | 1,300–850 | 2.63–2.57 | 8,860–8,660 |
| Io-B | 4 May 2016 | 22:32:30 | 3,000 | L, N, and U2 | 20.25–33 | 0.34–0.21 | 1,210–750 | 2.50–2.42 | 8,850–8,560 |

^aL, N, U2, U3, and UT stand for the Long Wavelength Array station One (LWA1), Nançay Decameter Array (NDA), URAN2, URAN3, and UTR2 radio telescopes, respectively. ^bThe east-west angular size and effective baseline are given by equations (1) and (2), respectively. The maximum values are in a pair of either LWA1-UTR2 or LWA1-URAN2, whichever is available. Similarly, the minimum values come from a pair of URAN2-UTR2, NDA-URAN3, or NDA-URAN2. ^c The lower common frequency is 16.5 MHz for the pairs of NDA-URAN3 and LWA1-URAN3, and 10.5 MHz for the other pairs.

et al., 1976; Nigl et al., 2007; Slee & Higgins, 1963, 1966). In this study, we use the cross-correlation analysis technique described by Imai et al. (2016). First, because all spectrograms were recorded with different spectral and temporal intervals for the nine Io-DAM events (Table 1), we synchronize the observed values related to the Stokes I at every station in term of frequency and time. The intensity values are synchronized into the common temporal resolution of 1 ms by virtue of the Catmull-Rom spline, and the mean values are calculated into the common spectral resolution of 50 kHz. Second, the frequency-dependent cross-correlation function r_f is computed as

$$r_f(\tau) = \frac{P_{xy}}{\sqrt{\sum_t (x_f(t) - \bar{x}_f)^2} \cdot \sqrt{\sum_t (y_f(t) - \bar{y}_f)^2}}, \quad (3)$$

with

$$P_{xy} = \sum_t [(x_f(t) - \bar{x}_f) \cdot (y_f(t + \tau) - \bar{y}_f)] (\tau \geq 0) \quad (4)$$

$$= \sum_t [(x_f(t + |\tau|) - \bar{x}_f) \cdot (y_f(t) - \bar{y}_f)] (\tau < 0), \quad (5)$$

where τ is shifted temporal variable (lag time), t is temporal variable in one-second period, x_f and y_f are observed Stokes I for each frequency in decibels in either of the telescope pairs, and \bar{x}_f and \bar{y}_f are mean values of x_f and y_f . It is important to note that a positive τ means that the time of x_f is more delayed than that of y_f . The third process is to approximately correct the initial timings of UTR2, URAN2, and URAN3 using the man-made signals simultaneously detected by NDA since these timings were tagged as the DPS-Z

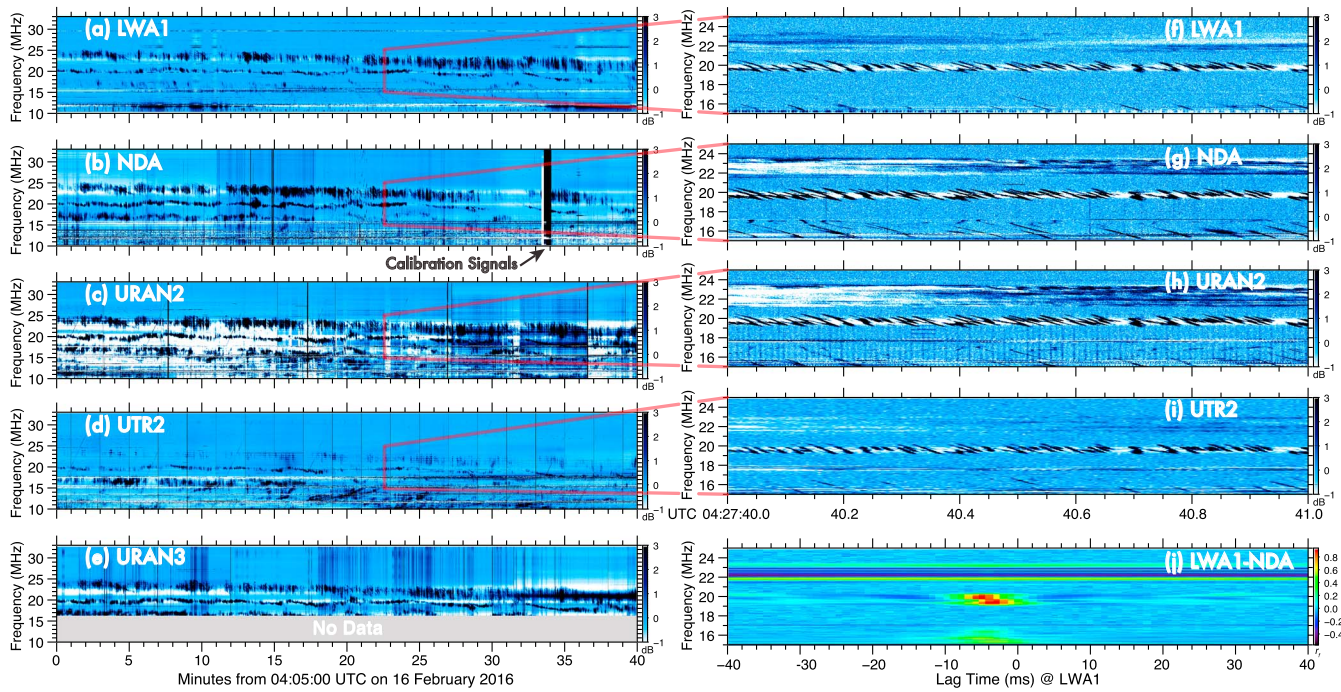


Figure 2. Coordinated Jovian Io-C observation with the (a) LWA1, (b) NDA, (c) URAN2, (d) UTR2, and (e) URAN3 radio telescopes on 16 February 2016. The 1-s dynamic spectra including a train of spiky S-bursts and smooth L-bursts are depicted for (f) LWA1, (g) NDA, (h) URAN2, and (i) URAN3, and the cross-correlation spectrum is displayed for (j) LWA1-NDA. LWA1 = Long Wavelength Array station One; NDA = Nançay Decameter Array.

clock. The DPS-Z clock signals were not properly synchronized with the GPS clock time in contrast to the well-calibrated timings of the LWA1 and NDA. More details on this time calibration can be found in Appendix A. After this adjustment, we deduce the mean (μ) and standard deviation (σ) of r_f in 1-s periods for each frequency and impose a condition that r_f of the lag time must be above the threshold of $\mu + z_{99.5\%}\sigma$, where $z_{99.5\%}$ corresponds to a 99.5% confidence interval of a Gaussian distribution. This final method reduces quasi-random background fluctuations and allows us to analyze the variations of lag times at high r_f for the purpose of measuring the S-burst beaming structures.

Figures 2a–2e outline the synchronized observations of Jupiter's Io-C radiation from LWA1, NDA, URAN2, UTR2, and URAN3, lasting for 40 min from 04:05:00 UTC on 16 February 2016. The lowest frequency of URAN3 was 16 MHz owing to an operation issue, but the coverage of the observed frequencies from the other radio telescopes starts from 10 MHz. In the 1-s interval beginning from 04:27:40.0, three strong radio components dominate in the frequency bands at 15–17 and 19–21 MHz as a train of S-bursts and at 21–24 MHz as a group of L-bursts at LWA1 in Figure 2f, NDA in Figure 2g, URAN2 in Figure 2h, and UTR2 in Figure 2i. Figure 2j shows an instance of the cross-correlation spectrum of these emissions from LWA1 in Figure 2f and NDA in Figure 2g. The lag time (τ_{\max}) at highest cross-correlation functions ranges from -3 to -4 ms for a train of S-bursts in 15–17 and 19–21 MHz. The values of cross-correlation functions for the former is lower than those for the latter because of the absence of some fragments of S-bursts. The cross-correlation function for the L-bursts between 21 and 24 MHz is low because the temporal variations of L-bursts are comparable to those of the terrestrial ionospheric plasma medium and the interplanetary medium, thereby leading to strongly modulated intensities at each station. This situation is in contrast to the S-bursts changing on the order of milliseconds, which can be ignored for the slow variations of both aforementioned media.

After we repeat this computation for the entire 40-min event and average the results into a bin of 1-ms lag time, Figure 3 shows the mean cross-correlation functions plotted as a function of lag time and elapsed time since 04:05:00 UTC in the pairs of LWA1-NDA, LWA1-URAN3, LWA1-URAN2, and LWA1-UTR2. Also, we exclude a bin in which the observed counts are below the points of 1% of total spectral channels in mitigating temporal variations of the background noise. For each plot, as the elapsed time increases, the peak of the cross-correlation functions shifts in the positive lag time. Table 3 shows the east-west angular size and effective baseline dependance on the start and stop time of the observation. Likewise, Figure 4

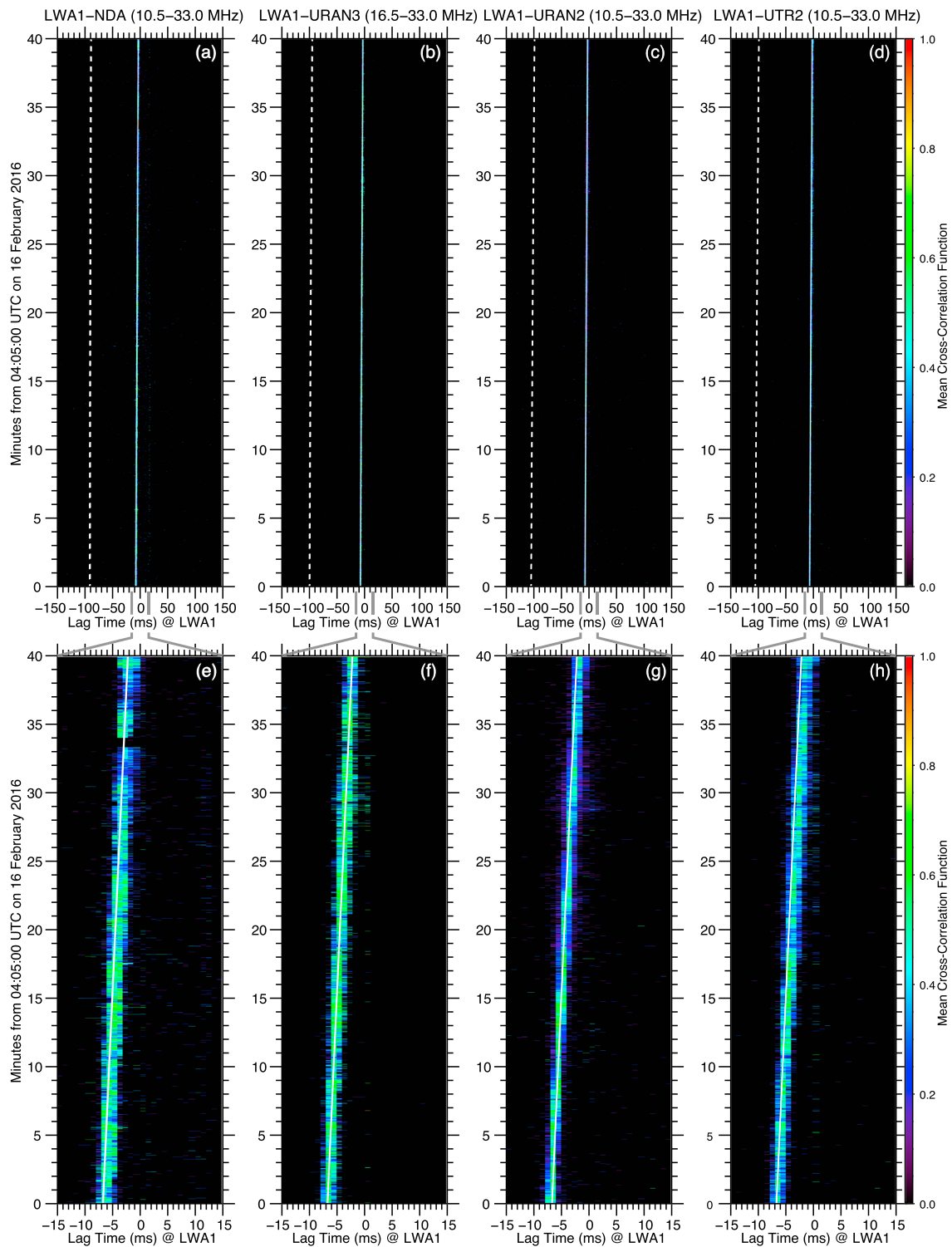


Figure 3. Mean cross-correlation functions depicted as a function of lag time and elapsed time from 04:05:00 UTC in the pairs (a, e) LWA1-NDA, (b, f) LWA1-URAN3, (c, g) LWA1-URAN2, and (d, h) LWA1-UTR2. The white solid and dotted lines correspond to the expected delay time calculated from the flashlight-like beaming and beacon-like beaming, respectively. LWA1 = Long Wavelength Array station One; NDA = Nançay Decameter Array.

Table 3
East-West Angular Size and Effective Baseline for Io-C on 16 February 2016

| Telescope pair | East-west angular size θ (") | | Effective baseline D (km) | |
|----------------|-------------------------------------|---------------------|-----------------------------|---------------------|
| | Start (04:05:00 UTC) | Stop (04:45:00 UTC) | Start (04:05:00 UTC) | Stop (04:45:00 UTC) |
| URAN2-UTR2 | 0.02 | 0.01 | 50 | 20 |
| URAN3-URAN2 | 0.15 | 0.11 | 480 | 360 |
| URAN3-UTR2 | 0.16 | 0.12 | 530 | 390 |
| NDA-URAN3 | 0.24 | 0.17 | 800 | 550 |
| NDA-URAN2 | 0.39 | 0.28 | 1,280 | 910 |
| NDA-UTR2 | 0.41 | 0.29 | 1,330 | 930 |
| LWA1-NDA | 2.33 | 2.40 | 7,620 | 7,840 |
| LWA1-URAN3 | 2.58 | 2.57 | 8,420 | 8,390 |
| LWA1-URAN2 | 2.72 | 2.68 | 8,900 | 8,750 |
| LWA1-UTR2 | 2.74 | 2.69 | 8,950 | 8,780 |

Note. LWA1 = Long Wavelength Array station One; NDA = Nançay Decameter Array.

displays Io-A/C, Io-A', Io-B, Io-C, and Io-B/D events using the pair of LWA1-URAN2 and shows the similar systematic trend as the Io-C event analysis.

3. Interpretation of Jovian S-Burst Beaming

The observed lag times can be accounted by either (1) flashlight-like or (2) beacon-like beaming of the Jovian radio sources as demonstrated in the work of Imai et al. (2016). In both models, we consider the longitudinal extent of these radio sources as localized within a narrow region because S-bursts are observable in a specific configuration of Jupiter and Io as seen from an observer (i.e., the box regions of Figure 1b). Model 1 has the radio sources distributed along a magnetic field line and emanating over large solid angles to the observer. In model 2, the radio sources emit over small solid angles along active magnetic flux tubes that are tied to Jupiter and Io as the planet rotates. The estimates of lag time from model 1 (τ_1) and model 2 (τ_2) can be expressed as

$$\tau_1 = \tau_{\text{prop}} + C, \quad (6)$$

$$\tau_2 = \tau_{\text{prop}} + \tau_{\text{rot}} + C \quad (7)$$

with C being the offset lag time, τ_{prop} being the propagation differential time between two telescopes, and τ_{rot} being the rotation lag time. The former comes from the timing corrections (Appendix A), and the latter two can be further described as

$$\tau_{\text{prop}} = (|\mathbf{a}| - |\mathbf{b}|) / c \quad (8)$$

$$\tau_{\text{rot}} = \frac{\theta[\text{rad}]}{\Omega_{\text{Jup}} - \Omega_{\text{Io}}} \quad (9)$$

where c is the speed of light, the notations of \mathbf{a} , \mathbf{b} , and θ are the same as in equations (1) and (2), and Ω_{Jup} ($870.536^\circ/\text{day}$) and Ω_{Io} ($203.489^\circ/\text{day}$) are angular velocities of Jupiter's System III rotation (cf. Riddle & Warwick, 1976) and of Io's orbital rotation (cf. Archinal et al., 2011), respectively. $\Omega_{\text{Jup}} - \Omega_{\text{Io}}$ represents angular velocity of Io's System III rotation, thereby carrying a possible active magnetic flux tube tied to Jupiter and Io.

Figures 3a–3d, illustrating for the Io-C S-burst event, show the mean cross-correlation functions in the range of -150 - to 150 -ms lag time, overlaid as the white solid line of τ_1 and the white dotted line of τ_2 . Clearly, there are no peaks of the mean cross-correlation functions along the τ_2 trend but it is certain along the τ_1 trend even in the range between -15 - and 15 -ms lag time in Figures 3e–3h. Likewise, Figures 4a–4h display eight examples, showing the white solid lines are overlapped with the peak of the mean cross-correlation functions. Note that the gaps in the cross correlations along the τ_1 trend are due to either no data from the

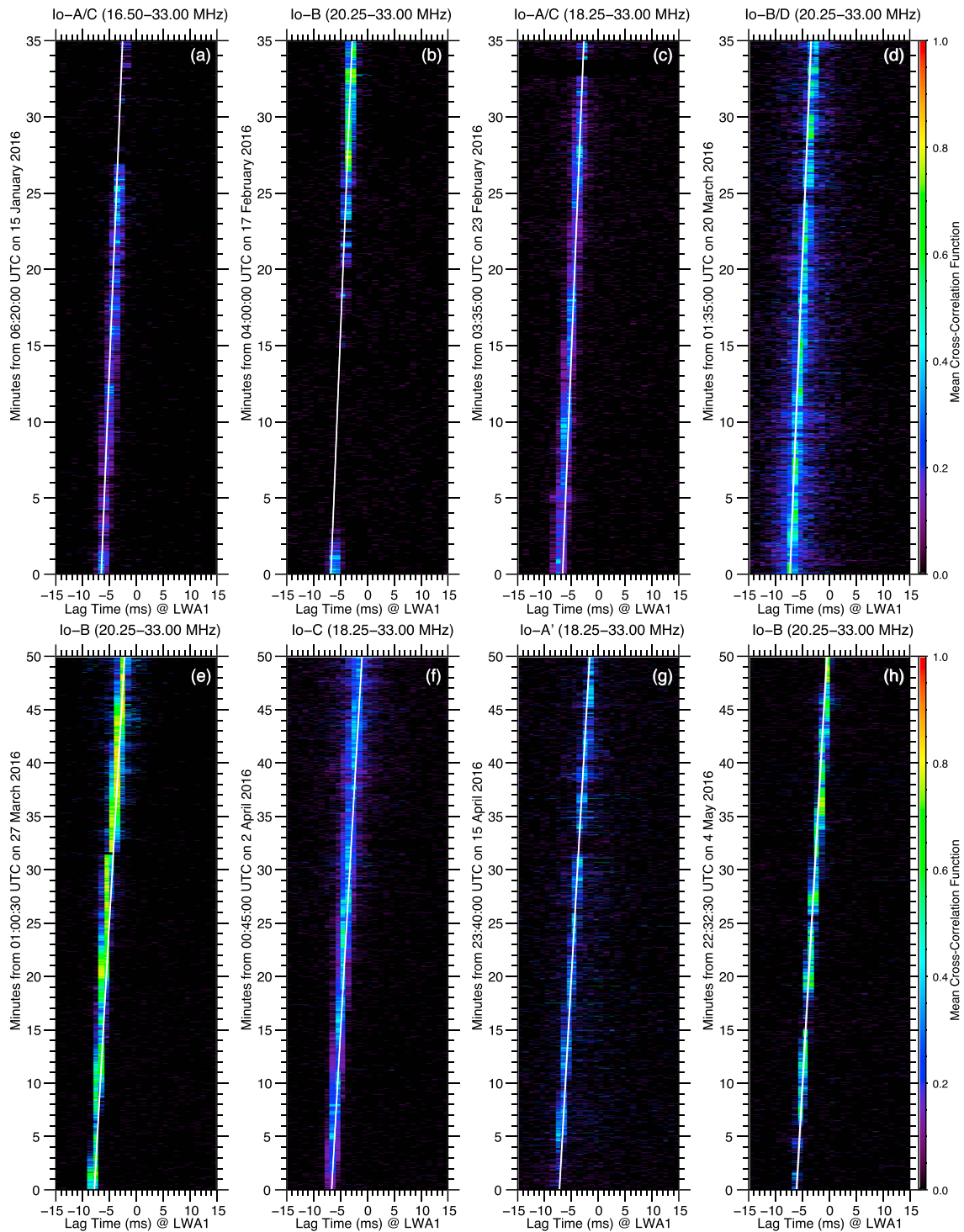


Figure 4. The format is the same as in Figure 3 but, in the pair of LWA1-URAN2, on (a) 15 January for Io-A/C, (b) 17 February for Io-B, (c) 23 February for Io-A/C, (d) 20 March for Io-B/D, (e) 27 March for Io-B, (f) 2 April for Io-C, (g) 15 April for Io-A', and (h) 4 May for Io-B. Note that the white dotted lines for the beacon-like beaming are outside of the lag time range in each plot. LWA1 = Long Wavelength Array station One.

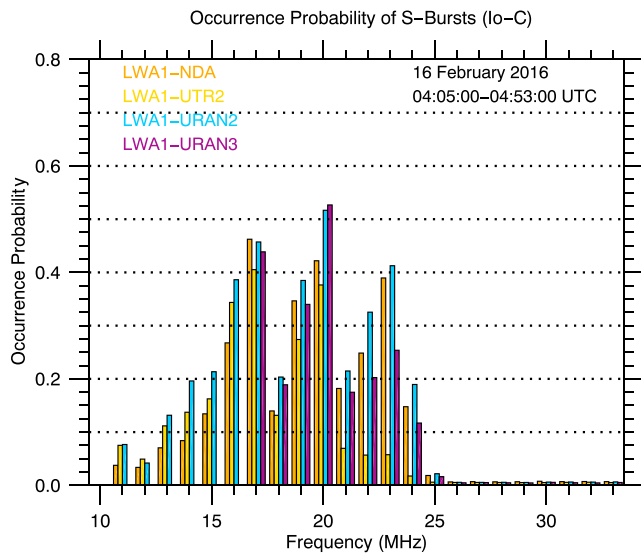


Figure 5. Using the cross-correlation technique, an occurrence probability histogram of S-bursts within the Io-C source on 16 February 2016 displayed as a function of frequency. The occurrence probabilities were integrated over the ± 1 -ms lag time with respect to the estimated τ_1 in Figure 3. NDA = Nançay Decameter Array; LWA1 = Long Wavelength Array station One.

electrons nonlinearly generate phase-coherent S-bursts as the interaction region moves upward along the active magnetic field lines near Io (Willes, 2002). The former model can only explain the simple negative drifting S-bursts, while the latter model is able to show the successful generations of both simple and complex S-bursts. From the observational point of view, we show that the active magnetic flux tubes are not synchronized with the motion of Io, which is a new constraint to improve further the above theoretical modeling.

A byproduct of the S-burst cross-correlation analysis gives frequency-dependent distributions of occurrence probability (Imai et al., 2016, 2018). Although nine Io-DAM S-burst events were examined, we focus on the Io-C event on 16 February 2016, where all of the available radio telescopes were operated in a broad frequency band from 10.5 to 33 MHz. While our cross-correlation analysis allows to extract coherent radiation on the time scale of milliseconds from two stations, including S-bursts and man-made fine emissions (in Appendix A), the latter can be easily removed if we use long baseline common observations with two distant pairs. Figure 5 shows a Jovian S-burst occurrence probability histogram, in which the bars are the integrated number of occurrences within ± 1 ms of the τ_1 trend, organized into a 1-MHz bin from the pairs of LWA1-NDA (orange), LWA1-UTR2 (yellow), LWA1-URAN2 (blue), and LWA1-URAN3 (purple). All pairs except for the LWA1-UTR2 pair display three peaks at 17, 20, and 23 MHz. A lack of 23-MHz peak in the LWA1-UTR2 pair was due to a sidelobe UTR2 beam at a low elevation of 9° to 16° . The high-occurrence probabilities at 17, 20, and 23 MHz are all S-bursts, which was supported from the Voyager radio observations of the Io-C source emissions (Leblanc & Genova, 1981). These three peak features are referred to as the narrowband splitting events (Leblanc & Rubio, 1982) or striated spectral activities (Thieman et al., 1988). Our cross-correlation technique clearly demonstrated an abundance of the S-burst emissions at 17, 20, and 23 MHz during the analyzed Io-C event.

4. Conclusion

This paper reports the results of the cross-correlation analysis for nine Jovian Io-related DAM S-bursts during the observation campaign in 2016 using several radio telescopes over effective baselines of up to 8,950 km. These telescopes include the Long Wavelength Array station One (LWA1) in the United States, Nançay Decameter Array (NDA) in France, and three large radio telescopes (UTR2, URAN2, and URAN3) in Ukraine. On the basis of the trend of the mean cross-correlation functions in each distant pair of the telescopes, we tested whether the S-burst beaming forms a narrow source distribution

LWA1 or no emissions during the observing periods. Therefore, the results of all nine examples support the flashlight-like model and constrain the beaming thickness to $2.75''$ for Io-A/C, $2.63''$ for Io-A', and $2.75''$ for Io-B/D in the east-west direction as viewed from Earth. Furthermore, the lag times measured in all usable pairs support the flashlight-like beam model, thereby leading to the conclusion that the beam was completely filled as seen from Earth.

Although the spectral morphology and the theoretical interpretations of S-bursts are diverse among the Io-DAM emissions, our observational finding shows that any S-bursts ubiquitously form the flashlight-like structure and removes the possibility of dragging active magnetic flux tubes connecting Io and Jupiter. The Io-B and Io-C L-burst arcs show the spectral shape like an open parenthesis, and those of Io-A, Io-A', and Io-D exhibit like a close parenthesis (Carr et al., 1983; Marques et al., 2017) owing to the emission beam geometry and different System III location of each radio source along complex magnetic field lines on Jupiter's polar regions (Connerney et al., 2018). More complicated, various kinds of S-bursts appear in each Io-DAM spectrogram characterizing the drift rate, emission frequency bandwidth, and interpulse intervals (Flagg et al., 1991; Riihimaa, 1992). One of the theoretical models is that the kinetic energy of weakly relativistic electrons is converted into the S-burst energy via CMI as their electrons move upwards along the Io flux tubes (Ellis, 1974; Zarka et al., 1996). Another model is that phase-bunching electrons

simultaneously coming from Jupiter in large solid angles (flashlight-like model) or a localized distribution with small solid angle directivity tied to Io's orbital motion in Jupiter's rotation frame (beacon-like model). The results for all nine Io-related events supported the former model is more favorable than the latter model, in agreement with Lynch et al. (1976) for the Io-B source and Imai et al. (2016) for the Io-D/B sources. It is emphasized that the number of examined events is very limited with only one event for Lynch et al. (1976) and (Imai et al., 2016), and it was unclear if their conclusions were generally consistent for the other cases of the Io-related events. Furthermore, according to the agreement for the flashlight-like model with various baselines using five different distant telescopes, we concluded that the Jovian S-burst beam was completely filled as viewed from Earth. The physical interpretation of the flashlight-like model is that an individual S-burst beam of a source coherently remains on the order of milliseconds and then completely disappears. This situation continuously repeats during the S-burst Io-DAM events. As originally pointed out by Lynch et al. (1976), this picture is in contrast to the L-burst beam forming as a beacon-like model, which is influenced by Io's orbital motion for Io-DAM (Kaiser et al., 2000; Panchenko & Rucker, 2016) and Jupiter's diurnal rotation for some of non-Io-related DAM (Imai et al., 2017).

Another benefit of this multi-instrument study provides S-burst frequency-dependent distributions isolated from those of L-bursts and man-made noises. A conventional way to find this discrepancy is either a visual survey of Jovian spectrograms in short periods (e.g., Flagg et al., 1991; Riihimaa, 1992) or a computer algorithm to extract only simple S-bursts (Zarka et al., 1996). In this study, we applied our cross-correlation technique for an Io-C event collected with all of the telescopes, and we found that three peaks at 17, 20, and 23 MHz correspond to the narrow-band splitting events (Leblanc & Rubio, 1982) or striated spectral activities (Thieman et al., 1988). Therefore, this technique is a practical tool to deepen our understanding of S-burst source distributions.

The cross-correlation analysis yields a new constraint on the minimum cone thickness of 2.75" for Io-A/C, 2.63" for Io-A', and 2.75" for Io-B/D in the east-west direction, as opposed to the much larger L-burst thickness of 1° (Kaiser et al., 2000; Panchenko & Rucker, 2016). This difference is not physical but an instrumental limitation on the usable baselines on Earth, while the long baseline analyses of concurrent Jovian L-bursts were performed by two distant spacecraft in space (Kaiser et al., 2000; Panchenko & Rucker, 2016). Interestingly, the upper bound of the source size for two emissions is comparable as estimated by 20 to 400 km for S-burst (Dulk, 1970; Zarka et al., 1996) and 70 km for L-burst (Imai et al., 1997).

Expanding the baseline beyond Earth provides a benefit to further constrain the size of the S-burst beam thickness. For example, there are numerous conceptual or planned missions around world to deliver a low-frequency radio system located near the Lunar orbit or on the Moon. One of them is Chinese Chang'E-4 mission, a series of the national Lunar projects, consisting of a relay satellite, a lander, and a rover (Jia et al., 2018). The relay satellite and the lander and rover set were launched on 20 May and 7 December 2018, respectively. Both the relay satellite and the lander are equipped with the low-frequency radio system that covers the entire Jovian DAM frequencies up to 40 MHz. Taking advantage of the 400,000-km baseline between Earth and Moon when the Earth-Jupiter distance is 4.2 AU, collecting Jovian S-bursts from Earth and Moon will be well suited to test if the cone thickness is larger than the angular resolution of 131".

Meanwhile, the Juno spacecraft has, since its arrival at Jupiter on 5 July 2016, monitored "near-field" in situ observations of Jovian polar auroras from a vantage point (Bolton et al., 2017; Connerney et al., 2017; Kurth et al., 2017). The Waves instrument (Kurth et al., 2017) is one of Juno's nine on-board instruments, specialized for observing the electric field waves from 50 Hz to 41 MHz and the magnetic field waves from 50 Hz to 20 kHz. Waves is capable of recording the time domain waveforms in a 1.3-MHz bandwidth at a central frequency tunable above 3 MHz (tracking the local gyrofrequency based on Juno's magnetometer (Connerney et al., 2017)), covering much of isolated groups of the S-burst radio spectrum. In concert with Juno's Waves observations, the ground-based "far-field" wave observations have been coordinated (e.g., Imai et al., 2017). Therefore, comparing S-bursts with Juno and ground-based radio telescopes will give an insight into multidimensional structures of the radio source and beam, but this remains for a further study.

Appendix A: Approximate Timing Correction of the Ukrainian Radio Telescopes Using Man-Made Radio Signals Commonly Recorded With NDA in France

To estimate the S-burst beam characteristics, it is imperative that all coordinated radio telescopes be precisely calibrated in time. The modern radio telescopes like LWA1 and NDA implement the GPS clock time to adjust their samples of records with an accuracy of better than 1 ms. In contrast, the Ukrainian radio telescopes (UTR2, URAN2, and URAN3) record the observed signals with the DSP-Z receiver time, not the GPS synchronized clock time in 2016. On Earth, the man-made signals are prevalent in the lower-frequency range below 40 MHz, which are simultaneously detected by NDA, another European radio station used in this study. Figure A1 illustrates a typical example of the man-made signals in the spectrograms of NDA and URAN2. The dual sweeping signals originate from the European Ionosonde stations. Assuming the ionospheric soundings from the 10 operating Ionosondes in Europe (Belehaki et al., 2015), the expected delay time varies from 1 to 8 ms. Another modulated man-made intensity signal appears at 10.3 MHz, which has a similar amount of propagation lag time. This example shows the lag time of 0.204 s at the peak of the cross-correlation function. Since the receiver time is also drifting in time, the lag time at the high cross-correlation function shows the linear trend, so that we can model this lag time tendency by constraining it with a least squares method. This was done for UTR2 and URAN3.

After this time adjustment, Figure A2 shows a result of the cross-correlation analysis for the Io-C event in the pairs of NDA-URAN3, NDA-URAN2, NDA-UTR2, URAN2-UTR2, URAN3-URAN2, and URAN3-UTR2 as a function of lag time and elapsed time from 04:05:00 UTC on 16 February 2016. The peak of the mean cross-correlation functions including the Jovian S-burst time evolution clearly shows a linear trend around 0-ms lag time. It is important to note that Figure A2 can be tested to disentangle two kinds of Jovian radio beaming as discussed in section 3. For all plots besides A2d, the white solid line from the flashlight-like model gives reasonable fits with the observed lag time in contrast to the white dotted line from the beacon-like model. Because the lag times estimated from both models in Figure A2d are very close each other around 0-ms lag time, this plot alone is unable to show which model is superior. However, owing to the favorable flashlight-like model from the other plots of Figure A2, the beam is larger than a 0.01–0.41" east-west view of the telescopes according to Table 3, consistent with 2.74" in the longest baseline pair of LWA1-UTR2 in Figure 3.

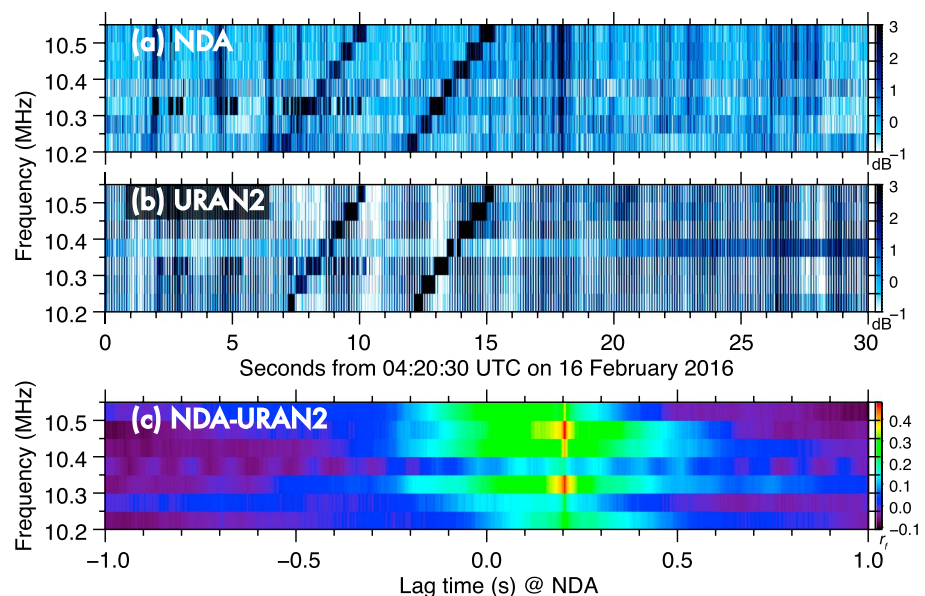


Figure A1. Synchronized spectrograms of man-made signals from (a) NDA and (b) URAN2 on 16 February 2016. There are two sweeping signals from the European Ionosonde stations and artificial intensity modulation at 10.3 MHz. (c) The cross-correlation spectrum of NDA-URAN2 is depicted as a function of lag time and frequency. NDA = Nançay Decameter Array.

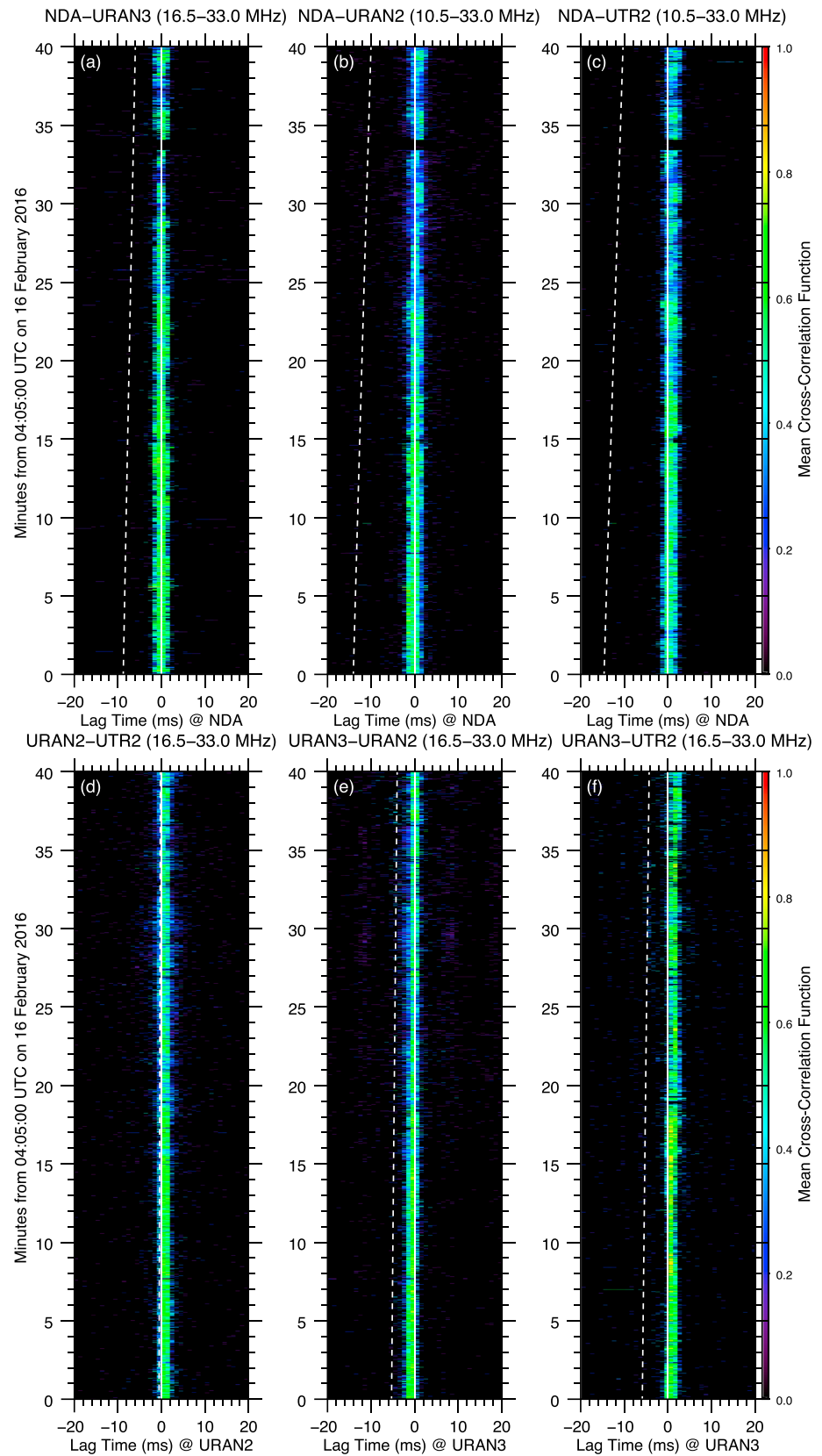


Figure A2. The format is the same as Figures 3e–3h but in the pairs of (a) NDA-URAN3, (b) NDA-URAN2, (c) NDA-UTR2, (d) URAN2-UTR2, (e) URAN3-URAN2, and (f) URAN3-UTR2. NDA = Nançay Decameter Array.

Acknowledgments

The authors are indebted to the engineers and staff who operate the LWA1, NDA, UTR2, URAN2, and URAN3 radio telescopes. They are grateful to K. Imai and L. Denis for providing the LWA1 and NDA telescope pictures in Figure 1a. They also appreciate the reviewers for fruitful comments and their careful reading of the manuscript. M. I. would like to thank L. J. Granroth and C. W. Piker of the University of Iowa for their kind assistance on the data compilation of ground-based radio telescopes. Basic research in radio astronomy at the Naval Research Laboratory is funded by 6.1 Base funding. Construction of the LWA has been supported by the Office of Naval Research under Contract N00014-07-C-0147. Support for operations and continuing development of the LWA1 is provided by the National Science Foundation under Grants AST-1139963 and AST-1139974 of the University Radio Observatory program. This research was initiated while one of the authors (M. I.) was a graduate student at Kyoto University, Japan. The LWA1 Jupiter data used in this study (project code LI001) were provided by the LWA team at University of New Mexico, which can be reachable via the project website at the University of Iowa (<https://space.physics.uiowa.edu/earth/>). Also, the other high-resolution data used for this publication are accessible at the same website.

References

Archinal, B., A'Hearn, M., Bowell, E., Conrad, A., Consolmagno, G., Courtin, R., et al. (2011). Report of the IAU working group on cartographic coordinates and rotational elements: 2009. *Celestial Mechanics and Dynamical Astronomy*, *109*(2), 101–135. <https://doi.org/10.1007/s10569-010-9320-4>

Belehaki, A., Tsagouri, I., Kutiev, I., Marinov, P., Zolesi, B., Pietrella, M., et al. (2015). The European Ionosonde Service: nowcasting and forecasting ionospheric conditions over Europe for the ESA Space Situational Awareness services. *Journal of Space Weather and Space Climate*, *5*, A25. <https://doi.org/10.1051/swsc/2015026>

Bigg, E. K. (1964). Influence of the satellite Io on Jupiter's decametric emission. *Nature*, *203*, 1008–1010. <https://doi.org/10.1038/2031008a0>

Boischoit, A., Rosolen, C., Aubier, M. G., Daigne, G., Genova, F., Leblanc, Y., et al. (1980). A new high-gain, broadband, steerable array to study Jovian decametric emission. *Icarus*, *3*, 399–407. [https://doi.org/10.1016/0019-1035\(80\)90185-2](https://doi.org/10.1016/0019-1035(80)90185-2)

Bolton, S. J., Lunine, J., Stevenson, D., Connerney, J. E. P., Levin, S., Owen, T. C., et al. (2017). The Juno mission. *Space Science Reviews*, *213*(1), 5–37. <https://doi.org/10.1007/s11214-017-0429-6>

Brazhenko, A. I., Bulatsen, V. G., Vashchishin, R. V., Frantsuzenko, A. V., Konovalenko, A. A., Falkovich, I. S., et al. (2005). New decameter radiopolarimeter URAN-2. *Kinematika i Fizika Nebesnykh Tel, Suppl.*, *5*, 43–46.

Brown, G. W., Carr, T. D., & Block, W. F. (1968). Long-baseline interferometry of S-bursts from Jupiter. *Astrophysical Letters*, *1*, 89–94.

Burke, B. F., & Franklin, K. L. (1955). Observations of a variable radio source associated with the planet Jupiter. *Journal of Geophysical Research*, *60*(2), 213–217. <https://doi.org/10.1029/JZ060i02p00213>

Carr, T. D., Desch, M. D., & Alexander, J. K. (1983). Phenomenology of magnetospheric radio emissions. In A. J. Dessler (Ed.), *Physics of the Jovian magnetosphere* (pp. 226–284). New York: Cambridge University Press.

Carr, T. D., Lynch, M. A., Paul, M. P., Brown, G. W., May, J., Six, N. F., et al. (1970). Very long baseline interferometry of Jupiter at 18 MHz. *Radio Science*, *5*(10), 1223–1226. <https://doi.org/10.1029/RS005i010p01223>

Clarke, J. T., Grodent, D., Cowley, S. W. H., Bunce, E. J., Zarka, P., Connerney, J. E. P., & Satoh, T. (2004). Jupiter's aurora. In F. Bagenal, T. E. Dowling, & W. B. McKinnon (Eds.), *Jupiter: The planet, satellites and magnetosphere* (pp. 639–670). New York: Cambridge University Press.

Clarke, T. E., Higgins, C. A., Skarda, J., Imai, K., Imai, M., Reyes, F., et al. (2014). Probing Jovian decametric emission with the Long Wavelength Array Station 1. *Journal of Geophysical Research: Space Physics*, *119*, 9508–9526. <https://doi.org/10.1002/2014JA020289>

Connerney, J. E. P., Adriani, A., Allegrini, F., Bagenal, F., Bolton, S. J., Bonfond, B., et al. (2017). Jupiter's magnetosphere and aurorae observed by the Juno spacecraft during its first polar orbits. *Science*, *356*(6340), 826–832. <https://doi.org/10.1126/science.aam5928>

Connerney, J. E. P., Benn, M., Bjarno, J. B., Denver, T., Espley, J., Jorgensen, J. L., et al. (2017). The Juno magnetic field investigation. *Space Science Reviews*, *213*, 39–138. <https://doi.org/10.1007/s11214-017-0334-z>

Connerney, J. E. P., Kotsiaros, S., Oliverson, R. J., Espley, J. R., Joergensen, J. L., Joergensen, P. S., et al. (2018). A new model of Jupiter's magnetic field from Juno's first nine orbits. *Geophysical Research Letters*, *45*, 2590–2596. <https://doi.org/10.1002/2018GL077312>

Dowell, J., Wood, D., Stoval, K., Ray, P. S., Clarke, T., & Taylor, G. (2012). The Long Wavelength Array software library. *Journal of Astronomical Instrumentation*, *1*(1), 1250006. <https://doi.org/10.1142/S2251171712500067>

Dulk, G. A. (1970). Characteristics of Jupiter's decametric radio source measured with arc-second resolution. *The Astrophysical Journal*, *159*, 671–684. <https://doi.org/10.1086/150341>

Dulk, G., Rayhrer, B., & Lawrence, R. (1967). The size of Jupiter's decametric radio source. *The Astrophysical Journal*, *150*, L117. <https://doi.org/10.1086/180105>

Ellingson, S. W., Taylor, G. B., Craig, J., Hartman, J., Dowell, J., Wolfe, C. N., et al. (2013). The LWA1 radio telescope. *IEEE Transactions on Antennas and Propagation*, *61*(5), 2540–2549. <https://doi.org/10.1109/TAP.2013.2242826>

Ellis, G. R. A. (1974). The Jupiter radio bursts. *Proceedings Astronomical Society of Australia*, *2*, 236–243.

Flagg, R., Greenman, W. B., Reyes, F., & Carr, T. D. (1991). *A catalog of high resolution Jovian decametric radio noise burst spectra* (Vol. 1). Gainesville, FL: University of Florida.

Gallet, R. M. (1961). Radio Observations of Jupiter. II. In G. P. Kuiper, & B. M. Middlehurst (Eds.), *Planets and satellites* (pp. 500–533). Chicago, Illinois: University of Chicago Press.

Imai, M., Kurth, W. S., Hospodarsky, G. B., Bolton, S. J., Connerney, J. E. P., Levin, S. M., et al. (2017). Latitudinal beaming of Jovian decametric radio emissions as viewed from Juno and the Nançay Decameter Array. *Geophysical Research Letters*, *44*, 4455–4462. <https://doi.org/10.1002/2016GL072454>

Imai, M., Lecacheux, A., Clarke, T. E., Higgins, C. A., Panchenko, M., Dowell, J., et al. (2016). The beaming structures of Jupiter's decametric common S-bursts observed from the LWA1, NDA, and URAN2 radio telescopes. *The Astrophysical Journal*, *826*(2), 176. <https://doi.org/10.3847/0004-637X/826/2/176>

Imai, M., Lecacheux, A., Clarke, T. E., Higgins, C. A., Panchenko, M., Dowell, J., et al. (2018). Erratum: “The Beaming Structures of Jupiter's Decametric Common S-bursts Observed from the LWA1, NDA, and URAN2 Radio Telescopes” (2016, ApJ, 826, 176 [<http://iopscience.iop.org/article/10.3847/0004-637X/826/2/176>]). *The Astrophysical Journal*, *862*(2), 175. <https://doi.org/10.3847/1538-4357/aad17f>

Imai, K., Wang, L., & Carr, T. D. (1997). Modeling Jupiter's decametric modulation lanes. *Journal of Geophysical Research*, *102*(A4), 7127–7136. <https://doi.org/10.1029/96JA03960>

Jia, Y., Zou, Y., Ping, J., Xue, C., Yan, J., & Ning, Y. (2018). The scientific objectives and payloads of Chang'E-4 mission. *Planetary and Space Science*, *162*, 207–215. <https://doi.org/10.1016/j.pss.2018.02.011>

Kaiser, M. L., Zarka, P., Kurth, W. S., Hospodarsky, G. B., & Gurnett, D. A. (2000). Cassini and Wind stereoscopic observations of Jovian nonthermal radio emissions: Measurement of beam widths. *Journal of Geophysical Research*, *105*(A7), 16,053–16,062. <https://doi.org/10.1029/1999JA000414>

Konovalenko, A., Sodin, L., Zakharenko, V., Zarka, P., Ulyanov, O., Sidorchuk, M., et al. (2016). The modern radio astronomy network in Ukraine: UTR-2, URAN and GURT. *Experimental Astronomy*, *42*(1), 11–48. <https://doi.org/10.1007/s10686-016-9498-x>

Kurth, W. S., Hospodarsky, G. B., Kirchner, D. L., Mokrzycki, B. T., Averkamp, T. F., Robison, W. T., et al. (2017). Juno Waves investigation. *Space Science Reviews*, *213*, 347–392. <https://doi.org/10.1007/s11214-017-0396-y>

Kurth, W. S., Imai, M., Hospodarsky, G. B., Gurnett, D. A., Louarn, P., Valek, P., et al. (2017). A new view of Jupiter's auroral radio spectrum. *Geophysical Research Letters*, *44*, 7114–7121. <https://doi.org/10.1002/2017GL072889>

Leblanc, Y. (1981). On the arc structure of the DAM Jupiter emission. *Journal of Geophysical Research*, *86*(A10), 8546–8560. <https://doi.org/10.1029/JA086iA10p08546>

Leblanc, Y., de La Noe, J., Genova, F., Gerbault, A., & Lecacheux, A. (1981). A catalogue of Jovian decametric radio observations from January 1978 to December 1979. *Astronomy and Astrophysics Supplement Series*, *46*, 135–149.

- Leblanc, Y., & Genova, F. (1981). The Jovian S burst sources. *Journal of Geophysical Research*, *86*(A10), 8564–8568. <https://doi.org/10.1029/JA086iA10p08564>
- Leblanc, Y., Gerbault, A., Denis, L., & Lecacheux, A. (1993). A catalogue of Jovian decametric radio observations from January 1988 to December 1990. *Astronomy and Astrophysics Supplement Series*, *98*, 529–546.
- Leblanc, Y., Gerbault, A., & Lecacheux, A. (1989). A catalogue of Jovian decametric radio observations from January 1982 to December 1984. *Astronomy and Astrophysics Supplement Series*, *77*, 425–438.
- Leblanc, Y., Gerbault, A., Lecacheux, A., & Boudjada, M. Y. (1990). A catalogue of Jovian decametric radio observations from January 1985 to December 1987. *Astronomy and Astrophysics Supplement Series*, *86*, 191–207.
- Leblanc, Y., Gerbault, A., Rubio, M., & Genova, F. (1983). A catalogue of Jovian radio observations from January 1980 to December 1981. *Astronomy and Astrophysics Supplement Series*, *54*, 135–148.
- Leblanc, Y., & Rubio, M. (1982). A narrow-band splitting at the Jovian decametric cutoff frequency. *Astronomy & Astrophysics*, *111*, 284–294.
- Lecacheux, A. (2000). The Nançay Decameter Array: A useful step towards giant, new generation radio telescopes for long wavelength radio astronomy. In R. G. Stone, K. W. Weiler, M. L. Goldstein, & J. L. Bougeret (Eds.), *Radio astronomy at long wavelengths* (pp. 321–328). Washington DC: AGU. <https://doi.org/10.1029/GM119p0321>
- Lecacheux, A., Konovalenko, A. A., & Rucker, H. O. (2004). Using large radio telescopes at decametre wavelengths. *Planetary and Space Science*, *52*(15), 1357–1374. <https://doi.org/10.1016/j.pss.2004.09.006>
- Lynch, M. A., Carr, T. D., & May, J. (1976). VLBI measurements of Jovian S bursts. *The Astrophysical Journal*, *207*, 325–328. <https://doi.org/10.1086/154496>
- Lynch, M. A., Carr, T. D., May, J., Block, W. F., Robinson, V. M., & Six, N. F. (1972). Long-baseline analysis of a Jovian decametric L burst. *Astronomy Letters*, *10*, 153–158.
- Marques, M. S., Zarka, P., Echer, E., Ryabov, V. B., Alves, M. V., Denis, L., & Coffre, A. (2017). Statistical analysis of 26 yr of observations of decametric radio emissions from Jupiter. *Astronomy & Astrophysics*, *604*, A17. <https://doi.org/10.1051/0004-6361/201630025>
- Nigl, A., Zarka, P., Kuijpers, J., Falcke, H., Bähren, L., & Denis, L. (2007). VLBI observations of Jupiter with the initial test station of LOFAR and the Nançay decametric array. *Astronomy & Astrophysics*, *471*(3), 1099–1104. <https://doi.org/10.1051/0004-6361:20077204>
- Panchenko, M., & Rucker, H. O. (2016). Estimation of emission cone wall thickness of Jupiter's decametric radio emission using stereoscopic STEREO/WAVES observations. *Astronomy & Astrophysics*, *596*(A18). <https://doi.org/10.1051/0004-6361/201527397>
- Phillips, J. A., Carr, T. D., Levy, J., & Greenman, W. (1988). 18 MHz interferometry of non-Lo-C L-bursts. In H. O. Rucker, S. J. Bauer, & B. M. Pedersen (Eds.), *Planetary radio emissions II* (pp. 69–78). Vienna: Austrian Academy of Sciences Press.
- Riddle, A. C., & Warwick, J. W. (1976). Redefinition of system III longitude. *Icarus*, *27*(3), 457–459. [https://doi.org/10.1016/0019-1035\(76\)90025-7](https://doi.org/10.1016/0019-1035(76)90025-7)
- Riihimaa, J. J. (1968). Structured events in the dynamic spectra of Jupiter's decametric radio emission. *The Astronomical Journal*, *73*, 265–270. <https://doi.org/10.1086/110627>
- Riihimaa, J. J. (1992). *Wide-range high-resolution S-burst spectra of Jupiter*. Oulu, Finland: University of Oulu.
- Rucker, H. O., Lecacheux, A., Konovalenko, A. A., & Leitner, M. (2001). New frontiers in decameter radio astronomy. In H. O. Rucker, M. L. Kaiser, & Y. Leblanc (Eds.), *Planetary radio emissions V* (pp. 51–62). Vienna: Austrian Academy of Sciences Press.
- Ryabov, V. B., Vavriv, D. M., Zarka, P., Ryabov, B. P., Kozhin, R., Vinogradov, V. V., & Denis, L. (2010). A low-noise, high-dynamic-range, digital receiver for radio astronomy applications: An efficient solution for observing radio-bursts from Jupiter, the Sun, pulsars, and other astrophysical plasmas below 30 MHz. *Astronomy & Astrophysics*, *510*, A16. <https://doi.org/10.1051/0004-6361/200913335>
- Slee, O. B., & Higgins, C. S. (1963). Long baseline interferometry of Jovian decametric radio bursts. *Nature*, *197*, 781–783. <https://doi.org/10.1038/197781b0>
- Slee, O. B., & Higgins, C. S. (1966). The apparent sizes of the Jovian decametric radio sources. *Australian Journal of Physics*, *19*, 167. <https://doi.org/10.1071/PH660167>
- Stannard, K. M., Dulk, G. A., & Rayhrer, B. (1970). Very long baseline interferometry of decametric radiation from Jupiter. *Radio Science*, *5*(10), 1271–1280. <https://doi.org/10.1029/RS005i010p01271>
- Taylor, G. B., Ellingson, S. W., Kassim, N. E., Craig, J., Dowell, J., Wolfe, C. N., et al. (2012). First light for the first station of the Long Wavelength Array. *Journal of Astronomical Instrumentation*, *1*(1), 1250004. <https://doi.org/10.1142/S2251171712500043>
- Thieman, J. R., Alexander, J. K., Arias, T. A., & Staelin, D. H. (1988). Striated spectral activity in Jovian and Saturnian radio emission. *Journal of Geophysical Research*, *93*(A9), 9597–9605. <https://doi.org/10.1029/JA093iA09p09597>
- Warwick, J. W., & Dulk, G. A. (1964). Faraday rotation on decametric radio emissions from Jupiter. *Science*, *145*(3630), 380–383. <https://doi.org/10.1126/science.145.3630.380>
- Willes, A. J. (2002). Jovian S burst drift rates and S burst/L burst interactions in a phase-bunching model. *Journal of Geophysical Research*, *107*(A5), 1061. <https://doi.org/10.1029/2001JA000282>
- Wu, C. S., & Lee, L. C. (1979). A theory of the terrestrial kilometric radiation. *The Astrophysical Journal*, *230*, 621–626. <https://doi.org/10.1086/157120>
- Zakharenko, V., Konovalenko, A., Zarka, P., Ulyanov, O., Sidorchuk, M., Stepkin, S., et al. (2016). Digital receivers for low-frequency Radio Telescopes UTR-2, URAN, GURT. *Journal of Astronomical Instrumentation*, *5*(4), 1641010. <https://doi.org/10.1142/S2251171716410105>
- Zarka, P. (1998). Auroral radio emissions at the outer planets: Observations and theories. *Journal of Geophysical Research*, *103*(E9), 20,159–20,194. <https://doi.org/10.1029/98JE01323>
- Zarka, P., Farges, T., Ryabov, B. P., Abada-Simon, M., & Denis, L. (1996). A scenario for Jovian S-bursts. *Geophysical Research Letters*, *23*(2), 125–128. <https://doi.org/10.1029/95GL03780>